Laser and Particle Beams (2008), *26*, 179–188. Printed in the USA.

doi:10.1017/S0263034608000207

Simulations of shock generation and propagation in laser-plasmas

I.G. LEBO,[1] A.I. LEBO,[2] D. BATANI,[3] R. DEZULIAN,[3] R. BENOCCI,[3] R. JAFER,[3] AND E. KROUSKY[4]

[1]Technical University–MIREA, Moscow, Russia
[2]Lomonosov Moscow State University, Moscow, Russia
[3]Dipartimento di Fisica "G. Occhialini," Università di Milano Bicocca, Milano, Italy
[4]PALS Research Centre, Prague, Czech Republic

(RECEIVED 6 October 2007; ACCEPTED 6 March 2008)

Abstract

We analyze the results of a recent experiment performed at the PALS laboratory and concerning ablation pressure at 0.44 μm laser wavelength measured at irradiance up to 2×10^{14} W/cm^2. Using the code "ATLANT," we have performed two-dimensional (2D) hydrodynamics simulations. Results show that 2D effects did not affect the experiment and also give evidence of the phenomenon of delocalized absorption of laser light.

Keywords: Ablation pressure; Delocalized absorption; Hydrodynamics simulations; Laser-driven shocks

INTRODUCTION

The process of laser ablation of low- and medium-*Z* targets is fundamental for laser-driven inertial confinement fusion (ICF) since it is the source of the driving pressure in ablative compression of fusion targets. Moreover, laser ablation has a wide range of applications (Bashir *et al.*, 2007, Bussoli *et al.*, 2007, Fang & Ahmad, 2007, Thareja & Sharma, 2006, Veiko *et al.*, 2006 Wang *et al.*, 2007). For this reason, very many studies of mass ablation rate and of the generation of ablation pressures have been carried out over the past 20 years. Despite this, there are still some good reasons to study the process of laser ablation today: (1) First, progress in laser technology and in laser smoothing techniques allow the realization of cleaner experiments. Most of past studies were done by focusing on small focal spots in order to achieve intensities $\geq 10^{13}$ W/cm^2. Thereby, results were affected by two-dimensional (2D) effects (lateral transport of thermal energy, lateral flow of mass).

Even when large spots were used, these were not optically smoothed (the first smoothing technique, random phase plates, was introduced in the 1980s (Kato *et al.*, 1984) and were then characterized by "hot spots." The measured ablation rate was therefore dominated by the effect connected to the short-scale nonhomogeneities.

Moreover, the use of phase zone plate optical smoothing (Stevenson *et al.*, 1994; Koenig *et al.*, 1994; Batani *et al.*, 1996, 2002) (see next section) allows a flat-top intensity distribution to be produced. This is important since the ablation parameters in the central flat region of the focal spot can be directly compared to analytical results obtained from one-dimensional (1D) models, which by definition assume a spatially uniform intensity. (1) At the shortest laser wavelengths, there is still some incertitude concerning the scaling versus laser intensity. For instance, measurements at 0.351 μm (Key et al., 1983, 1979) showed a scaling $\approx I^{0.3}$, very different from what is predicted by theoretical models (usually $\approx I^{0.7}$). Such experimental results were dominated by 2D and hot spots effects. This is important because shorter laser wavelengths (third and fourth harmonics of Nd, as well as other wavelengths from gas lasers) give higher ablation rate and pressure, and are thereby envisaged as future drivers for ICF direct drive experiment (Koenig *et al.*, 1992; Lindl, 1995). Also, this allows studying material characteristics (Fortov *et al.*, 2002) and plasma characteristics (Batani *et al.*, 1999, 2007). (3) Finally, still some details are not clear in the literature concerning the very mechanism of laser ablation. For instance, even recent important reviews (Lindl, 1995) report the scaling law:

$$P(\text{Mbar}) = 8.6(I/10^{14})^{2/3}\lambda^{-2/3}(A/2Z)^{1/3}, \quad (1)$$

Address correspondence and reprint requests to: D. Batani, Dipartimento di Fisica "G. Occhialini," Università di Milano Bicocca, Piazza della Scienza 3, 20126 Milano, Italy. E-mail: batani@mib.infn.it

where I is the laser intensity on target in W/cm^2, λ is the laser wavelength in μm, and A and Z are the mass number and the atomic number of the target. This is obtained if laser light is absorbed at the plasma critical layer.

In reality, the scaling should also include time dependence. The plasma corona becomes larger during the interaction, and the distance between the absorption region and the ablation surface ($n_e \approx$ solid material) increases with time. This brings to a decoupling of the laser beam from the target and, as a result, the mass ablation rate decreases with time. In particular, it is found that the shock pressure is related to laser and target parameters (Mora, 1982).

$$\mathrm{P(Mbar)} = 11.6(I/10^{14})^{3/4}\lambda^{-1/4}(A/2Z)^{7/16}(Z^*t/3.5)^{-1/8}, \qquad (2)$$

where the time t is in ns. As in Eq. (1), pressure strongly depends on laser parameters and only weakly on the material. The decrease in time of pressure, even for constant laser irradiation, has been first described by Caruso and Gratton (1968) and Mora (1982). The difference between de-localized absorption and localized (at critical density) models is discussed elsewhere (Gus'kov, 1983; Meyer & Thiell, 1984; Limpouch, 1987).

In order to address questions (1), (2), and (3), an experiment was recently performed at the PALS laboratory, using irradiation at $\lambda = 0.44$ μm (Batani *et al.*, 2003*a*). Results showed a scaling versus laser intensity quite close to the theoretical prediction and also gave some evidence for the mechanism of delocalized absorption.

Experimental details have been analyzed (Batani *et al.*, 2003*a*, 2003*b*). However, one question, which remained partially opened, was the possibility of 2D effects partially affecting the measurement of shock velocity in that experiment. The goal of this paper is therefore to support experimental results with 2D numerical hydrodynamical simulations performed with the code "ATLANT" (Lebo, 1994, 2004) and derive more detail scaling for future experiments.

EXPERIMENTAL SETUP AND RESULTS

The experiment was performed with the iodine laser of PALS (Jungwirth, 2005; Batani *et al.*, 2007), which delivers a single beam, 29 cm in diameter, with typical energy of 250 J per pulse at 0.44 μm (Jungwirth *et al.*, 2001). The laser pulse is Gaussian in time with a full width at half maximum (FWHM) of about 400 ps.

The focusing lens had a focal length $f = 600$ mm ($f/2$ aperture). A blue filter before the entrance window did cut ω and 2ω light. The diagnostics used to detect the shock breakout from the target rear face consisted in a pair of lenses imaging the rear face onto the slit of a streak camera (Hamamatsu C7700 with S-1 photocathode). The first one was a complex $f/2$ objective, with $f = 100$ mm, producing a parallel beam between the two lenses. The second lens had $f = 98$ cm, giving a total optical magnification $M = 9.8$.

Stepped targets were made of bulk Al by lathe matching. The base was ≈8 μm, and the step thickness was ≈8.5 μm. Al was chosen because its behavior at high pressure is well known, making it a typical reference material for laser-shock experiments.

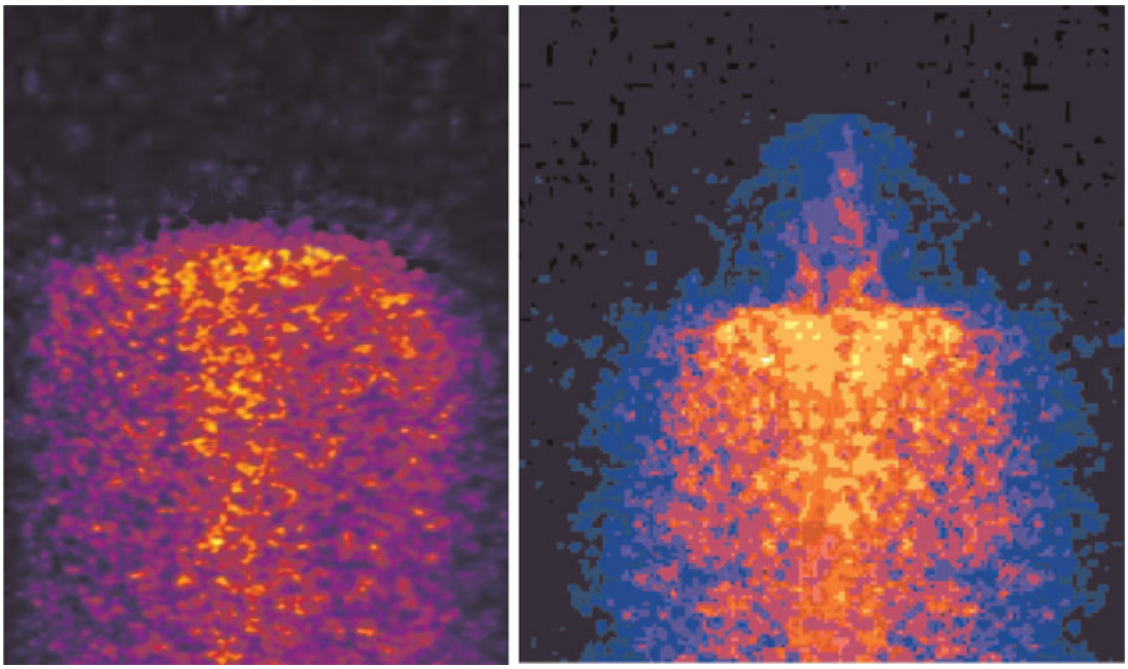

Fig. 1. (Color online) **Left:** shock breakout from a flat aluminum target. **Right:** Shock breakout image from an Al target for laser energy $E_L = 108$ J. The dimensions of the images are 1.69 ns × 1300 μm. Time flows up to down. Velocity of shock wave can be obtained as $D = d_2/(t_2 - t_1)$. Here the time delay between base and step is $\Delta t = (t_2 - t_1) = 267$ ps giving a shock velocity $D = 31.84$ μm/ns.

The primary condition of producing high quality flat shocks imposed the use of phase zone plates (PZP). Since, for technical reasons, it was not possible to produce a PZP with the full size of the laser beam, we designed a smaller PZP to be placed at $f/2$ from the target. The design of our optical system (PZP + focusing lens) implied a focal spot of 400 μm FWHM, with a 250 μm flat region in the center, corresponding to intensities up to 2×10^{14} W/cm^2.

Figure 1 shows a streak image of shock breakout from planar and stepped Al targets. The first image shows that a rather flat shock front has been created. The second image allows measuring the time delay between the breakout at the base and at the step, giving the average shock velocity in the step. From shock velocity we determine the shock pressure using the Hugoniot data for Al from the SESAME tables (T4 Group LANL, 1983). Such shock pressure is the pressure produced by the laser beam on the irradiated side, i.e., the ablation pressure.

The method works if the shock is stationary, and we designed the targets to get a stationary shock in the step. This can be addressed by using hydrodynamics simulations or analytical models (Batani *et al.*, 2001, 2003*c*), which approximates the Gaussian with a trapezoidal time shape, and again was checked by using the code "ATLANT."

SIMULATION CODE

We used the 2D hydrodynamic Lagrangian code "ATLANT" in cylindrical geometry (with coordinates R, z, t). Below we list the set of basic equations, which have been solved numerically with help of different methods (see in details in Lebo & Tishkin, 2006).

$$
\begin{aligned}
\frac{d\rho}{dt} &= -\rho\vec{\nabla}\vec{v} \\
\rho\frac{d\vec{v}}{dt} &= -\vec{\nabla}(Z_i \cdot P_E + P_I + P_R) \\
Z_i\rho\frac{dE_E}{dt} &= -Z_i \cdot P_E\vec{\nabla}\vec{v} + \vec{\nabla}(\kappa_E\vec{\nabla}T_E) - Q_{EI} \\
&\quad - Q_{ER} - R_{RAD}(\rho, T_E) + \vec{\nabla}\vec{q} \\
\rho\frac{dE_I}{dt} &= -P_I\vec{\nabla}\vec{v} + \vec{\nabla}(\kappa_I\vec{\nabla}T_I) + Q_{EI} \\
\rho\frac{dE_R}{dt} &= -P_R\vec{\nabla}\vec{v} + \vec{\nabla}(\kappa_R\vec{\nabla}T_R) + Q_{ER} \\
\left(\frac{\vec{q}}{|\vec{q}|}, \vec{\nabla}\right)\vec{q} &= k(\rho, T_E) \cdot \vec{q} \\
Q_{EI} &= Q_0(\rho, T_E)\frac{T_E - T_I}{T_E^{3/2}}\rho^2 \\
P_E &= P_E(\rho, T_E);\ P_I = P_I(\rho, T_I);\ P_R = P_R(\rho, T_R) \\
E_E &= E_E(\rho, T_E);\ E_I = E_I(\rho, T_I);\ E_R = E_R(\rho, T_R)
\end{aligned}
\tag{3}
$$

Here ρ is the density, ν is the velocity; E_E, E_I, E_R are the specific (i.e., per units of volume) internal energy of electrons, ions, and photons; P_E, P_I, P_R, T_E, T_I, T_R are the electron, ion, radiation pressures, and temperature; R_{RAD} represents the radiation losses of plasma; $\vec{q}$ is the laser-radiation flux; κ_E, κ_I, κ_R are the coefficients of thermal conductivity for the electron, ion, and radiation plasma components; Z_i is the mean degree of ionization in the Lagrange cell; k-is the absorption factor of laser radiation. Finally the following equations

$$
\begin{aligned}
Q_{EI} &= Q_{0EI} \cdot \frac{T_E - T_I}{T_E^{3/2}} \cdot Z_i\rho^2 \\
Q_{ER} &= Q_{0ER} \cdot \frac{T_E - T_R}{\sqrt{T_E}} \cdot Z_i\rho^2
\end{aligned}
\tag{4}
$$

give, respectively, the rate of electron-ion energy exchange in the Landau-Spitzer approximation, and the rate of electron-photon energy exchange, which is determined by the bremsstrahlung processes.

In our simulations, we have used a library for state equations based on the quotidian equations of state model (QEOS) (More *et al.*, 1988). It consisted of three parts: (1) Electron ionization-equilibrium equation of state based on Thomas-Fermi statistical model with scaling property for atomic number and atomic weight. (2) Analytical ion equation of state that combines Debye, Gruneisen, Lindemann and fluid-scaling laws. (3) Empirical term, which introduces correction for chemical bonding, and is derived from physical properties of a given material.

No radiation transport has been used in the simulation because we expect that this (and in particular, X-ray preheating) is negligible in our case, due to the sufficiently low laser intensity and to the use of a CH ablator before the Al layer.

SIMULATION RESULTS AND COMPARISON WITH EXPERIMENTAL DATA

We have performed several sets of simulations in order to reproduce the experimental results on measurement of shock wave velocity in stepped targets. In our simulations, we have varied the absorbed laser energy (E_{Las}^{abs}) from 50 to 200 J and the shape of the laser intensity profile ("Flat-top" or "Gauss") while keeping constant the laser wavelength (3ω, $\lambda = 0.438$ μm) and pulse duration. For simplicity, the temporal shape of the pulse was taken triangular, beginning at the time $t = 0$, having its maximum at $t = 400$ ps, and ending at $\tau = 800$ ps.

We have simulated the irradiation of three-layered disks: CH layer ($d_{CH} = 2$ μm), first Al layer ($d_{1\_Al} = 8$ μm) and second Al layer ($d_{2\_Al} = 8.5$ μm). Figure 2 shows the initial Lagrangian mesh, $0 < R < R_0$. On borders of the simulated area ($R_0 = 200$ μm) elastic and thermal isolated walls boundary conditions have been set. In order to avoid unnecessary numerical problems around the step edge, the base/step profile has been "smoothed" by assuming

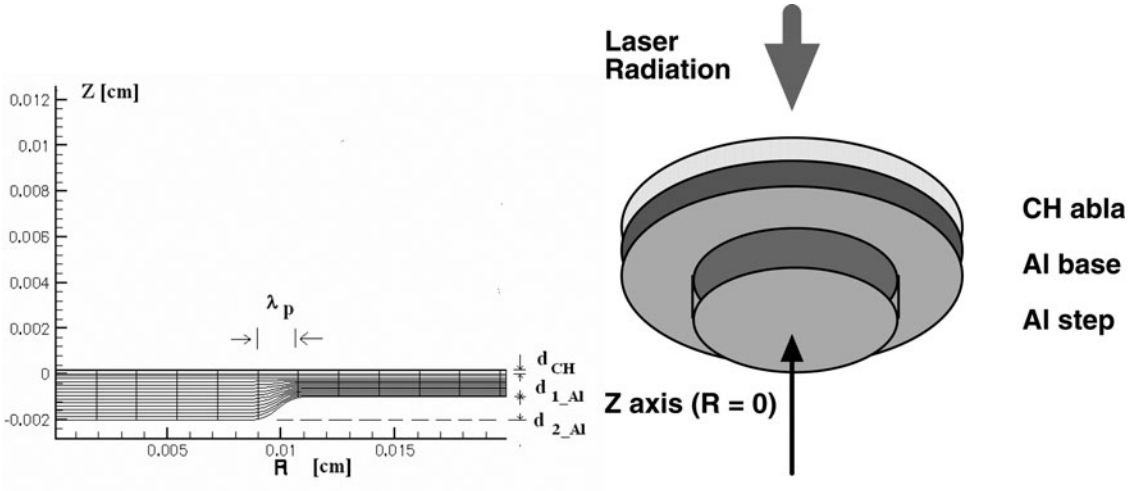

Fig. 2. Left: initial Lagrange mesh used in the ATLANT-code simulation (cylindrical symmetry around the Z axis is assumed), **Right:** scheme of the simulation.

a sinusoidal profile (over a typical half of wavelength of $\lambda_p =$ 20 μm), as it is clear from Figure 2.

The maximum laser intensity is $I_{max} = 2E_{las}^{abs}/\pi R_F^2 \tau$, where R_F is the radius of the focal spot. first case ($R_0 =$ 200 μm, absorbed energy 100 J): we first present the results of simulations with $R_F = R_0 = 200$ μm, and a "flat-top" laser flux profile.

Figures 3a and 3b shows the situation at the time when the shock reaches the rear side of the base, and at the time when it reaches the rear side of the step (notice the plasma corona expansion in the region $Z > 0$ and the part of the target which has been ablated). The simulation has been performed for a laser absorbed energy of 100 J, the shock reaches the rear side of the base $t_1 = 0.3257$ ns and it reaches the rear side of the step at $t_2 = 0.555$ ns. This gives a shock wave velocity $D = d_2/(t_2 - t_1) = 8.5$ μm/(0.555 ns – 0.3257 ns) = 37.07 km/s.

We have also made 1D calculation with help of "ATLANT" code to study if 2D geometry affects the shock wave velocity. The target consisted of two layers: outer CH layer with initial thickness 2 μm ($0 < Z < 2$ μm) and Al layer with thickness 16.5 μm (-16.5 μm $< z < 0$). The shock wave first reaches the CH-layer and part of the second layer with thickness 8 μm at the moment $t_1 = 0.328$ ns and reached the rear side of target at the moment $t_2 = 0.5576$ ns. These results are close to the 2D ones (with stepped targets). Figure 4 illustrates the density and pressure profiles at the time moments $t = 0.3226$ ns (1) and $t = 0.5576$ ns (2b). From these simulations, it follows that the transverse motion does not influence the measurement of shock wave velocity in condense matter and that $D = 37.1$ km/s too.

Second case ($R_0 = 200$ μm, absorbed energy 68 J): Figures 5a to 5d illustrate the density and pressure profiles in the z-direction at $R = 0$ (step) and at $R = 197.5$ μm (base).

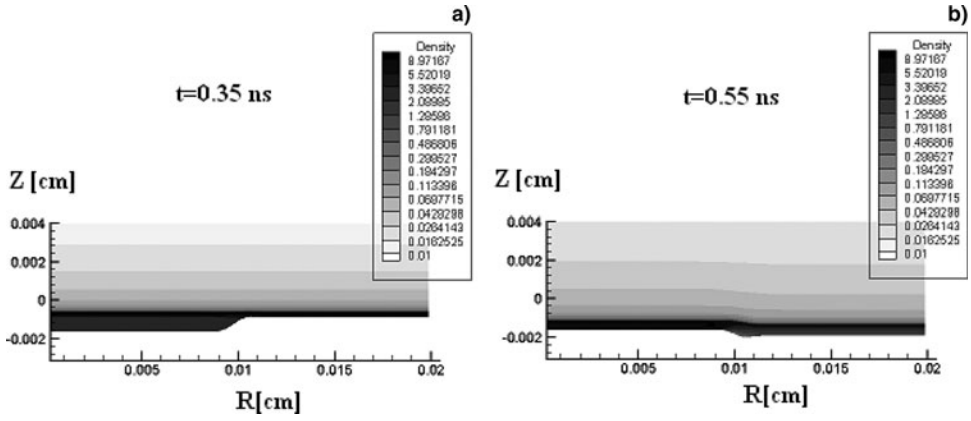

Fig. 3. The contours of target density at the time: (**a**) $t = 0.35$ ns (just after the shock reaches the rear of the base) and (**b**) $t = 0.55$ ns (just before it reaches the rear of the step). $E_{Las}^{abs} = 100$ J. The laser beam comes from top of figure.

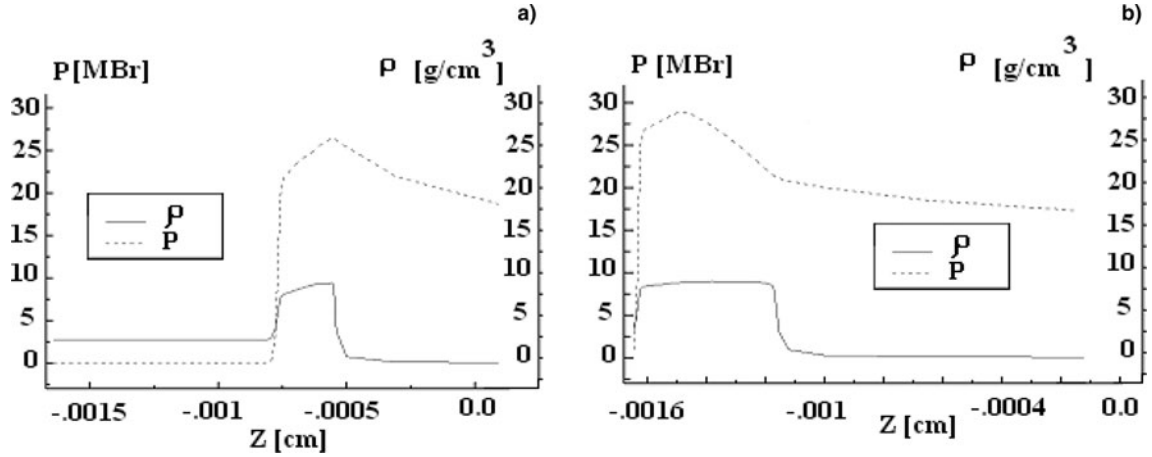

Fig. 4. Density and pressure profiles at $t_1 = 0.3226$ ns (shock front has reached the base-step interface at $Z = -8$ μm) (**a**) and $t_2 = 0.5576$ ns (shock front has reached the rear side at Z = −16.6 μm) (**b**) in 1D simulation. $E_{Las}^{abs} = 100$ J.

In this case, the shock wave reaches the first boundary $t_1 = 0.37$ ns and the second boundary at $t_2 = 0.619$ ns. Figure 5 shows the density profile (1) and the pressure profile (2) at $t_1 = 0.4$ ns, just after the shock wave has come to the rear side of the base; and the density (3), and pressure (4) profiles at $t_2 = 0.65$ ns just after it has reached the rear of the step, and the right part of target is unloaded.

Third case ($R_0 = 100$ μm, laser intensity 4×10^{14} W/cm^2): The distance, which the shock wave travels in condense matter is much less then the transverse scale of target R_0 and

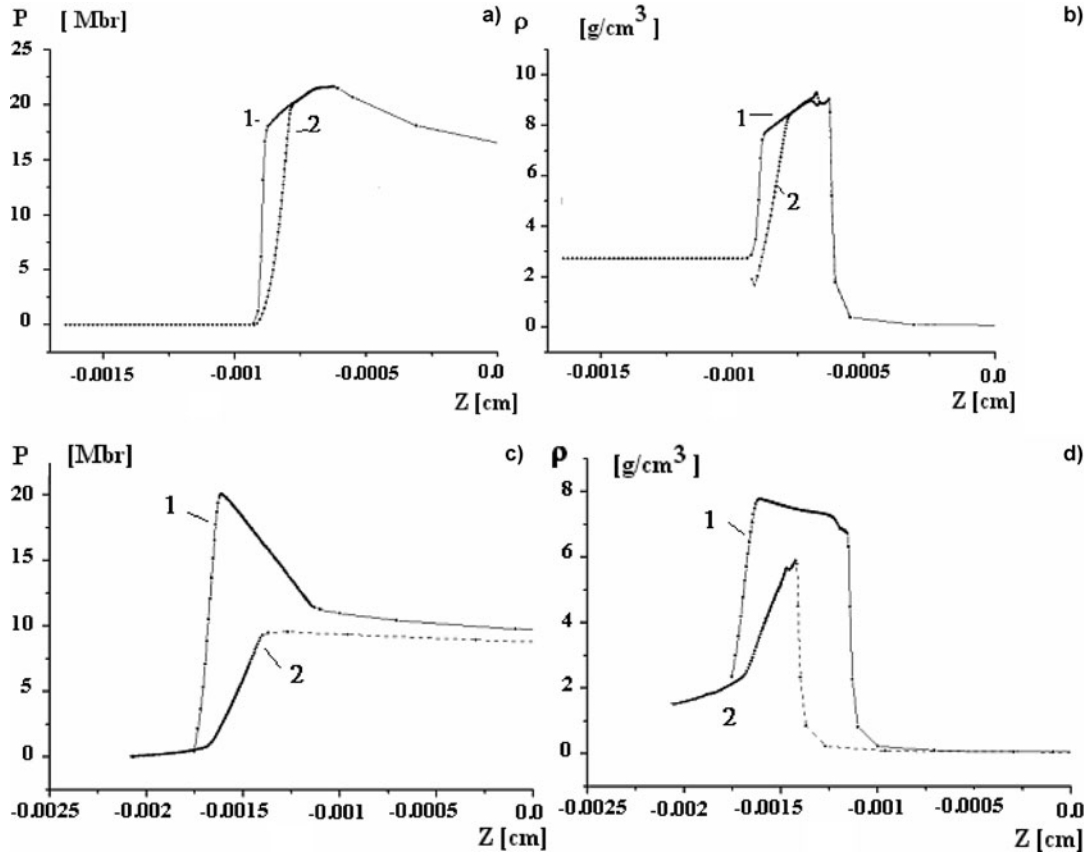

Fig. 5. 2D simulations: density (**a**) and pressure (**b**) profiles at $t = 0.4$ ns (0.03 ns after shock breakout at the base); density (**c**) and pressure (**d**) profiles at $t_2 = 0.65$ ns (0.03 ns after shock break out at the step); $E_{Las}^{abs} = 68$ J. (1) profile at $R = 0$ (Z axis), and (2) at $R = 197.5$ μm.

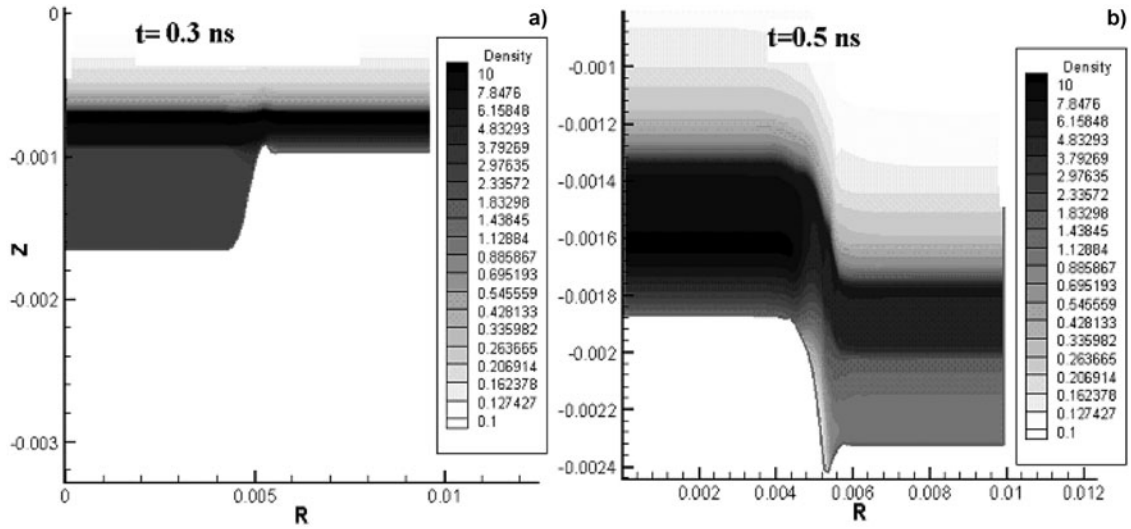

Fig. 6. Maximal laser intensity $I_{max} = 4 \times 10^{14}$ W/cm^2: the shock wave reaches the rear side of the base at $t_1 = 0.274$ ns and the step at $t_2 = 0.467$ ns. The case (**a**) shows the situation at $t = 0.3$ ns, and the case (**b**) at $t = 0.5$ ns.

mainly depends on laser intensity. In another simulation, we have diminished R_0 by two times and used $I_{max} = 4 \times 10^{14}$ W/cm^2. Figure 6 illustrates the motion of shock wave in the target. In this case, we got $D = 44$ km/s.

DISCUSSION

Figure 7 illustrates the results of a set of numerical simulations for the different values of I_{max}. We have compared the numerical results of shock wave velocities with experimental data. The "crosses" are the experimental data, the solid line is the results of simulations. In our simulations, we assumed a 100% absorption of laser energy. In the real experiment, part of the energy was lost as a result of the use of PZPs, of partial absorption of the e.m. wave in the plasma and of (2D) refraction effects in the plasma corona. As a result, we expect simulation results to be an upper limit to the experimental data, as it is indeed the case in Figure 7. We have supposed that about 30% of laser energy was lost.

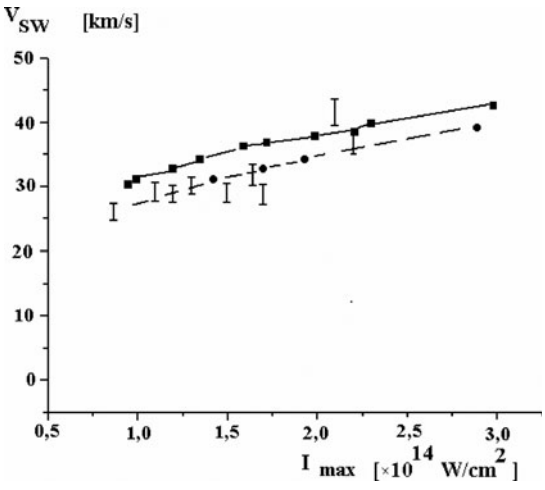

Fig. 7. Shock velocity vs. incident laser intensity, markers (I): experimental points after (Batani et al. 2003*a*), continuous line with markers (▪): simulation results, dashed line with markers (•), – corrected results with take into account the losses of laser energy.

In a second series of calculations, we studied the issue of conformity of data "scaling: to Eqs. (1) and (2). For this purpose, we simulated the interaction of laser light with an Al layer with initial thicknesses $d = 20-60$ μm without step profile with a flat-top laser profile with radius 200 μm. Thus, 2D effects were not considered.

The temporal shape of the laser pulse was an isosceles triangle reaching zero at times $t_1 = 0$ ns and $t_3 = 0.8$ ns with maximum at $t_2 = 0.4$ ns. In the calculations, the effects of laser beam refraction and reflection were not considered, and again we assumed 100% absorption of laser radiation in plasma. The profiles of pressure and density along the Z axis at the different time moments comes from our calculations. The maximum of pressure value has been increased up to $t = 0.4$ ns.

In this series of simulations, in addition to the QEOS model, we also used the equation of a state (EOS) proposed in Zel'dovich and Raizer (1967) and Afanas'ev *et al.* (1982), which considers two terms in the equation of ionic pressure: the thermal and the elastic factor, which calculates the ionization kinetics with an average ion approach in each Lagrangian cell. This is described by the following sets of equations

$$\begin{aligned} &P_i = P_{Ti} + P_{el}, \quad P_{Ti} = nT, \\ &P_{el} = \rho_0 C_S^2 \begin{cases} (\rho/\rho_0)^{ZN} - 1, & if \quad (\rho/\rho_0) \geq 0 \\ 0, & if \quad (\rho/\rho_0) < 0 \end{cases} \\ &P_e = ZnT, \quad \rho = m_i \cdot n \\ &\frac{dZ}{dt} = Z \cdot (\varphi_i - \varphi_r - \varphi_{fr}). \end{aligned} \tag{5}$$

Table 1. *Maximum pressure in the case $\lambda = 0.438$ μm $t = 0,4$ ns versus laser intensity. Second line: numerical calculations using the QEOS model; third line: numerical calculations using the RZI model; fourth line: analytical scaling using Eq. (2)*

I [10^{14} W/cm^2]	0.995	1.49	1.99	2.985	3.98	7.96
P_{QEOS} [MBar]	16.06	22.50	28.56	39.98	50.76	90.25
P_{ZRI} [MBar]	15.80	23.80	30.50	39.10	46.50	94.20
P_s [MBar]	16.06	23.34	28.56	39.98	50.77	90.25

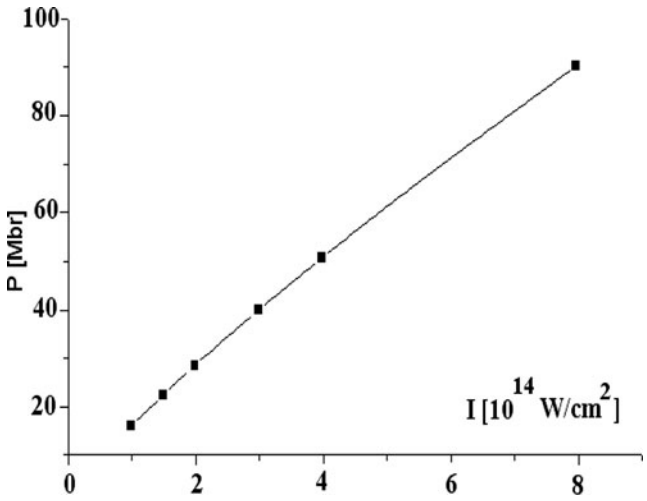

Fig. 8. Dependence of pressure on maximum laser intensity at $\lambda = 0.438$ μm and at $t = 0.4$ ns.

Here ρ and n are the density and ion concentration in condense matter, Z is the average ion charge in the Lagrangian cell, φ_i, φ_r, and φ_{fr} are the rates of three particle ionization, three particle-recombination and photo-recombination, and ρ_0 and C_s are the initial density and sound velocity in condense matter in normal conditions.

Calculations have been made for various values of laser intensity (I_{max}) at a fixed wavelength $\lambda = 0{,}438$ μm (see Table 1). From numerical calculations it is possible to derive the following scaling which is valid for the case $\lambda = 0.438$ μm.

$$P_S[MBar] = 16.22 \cdot \left(\frac{I}{10^{14}[W/cm^2]}\right)^{0,83}. \quad (6)$$

This shows a power dependence on laser intensity, which is quite close to the that of Eq. (2), the exponent being 0.83 instead of 0.75 (the difference with the exponent in Eq. (1), which is 0.67 is far more pronounced).

Figure 8 illustrates the results contained in Table 1 showing the results of numerical calculations of maximum pressure (P_{max}) versus intensity at the fixed wavelength of laser radiation $\lambda = 0.438$ μm (3ω).

In the case of the Zel'dovich and Raizer (1967) model with ionization kinetics (ZRI-model), the dependence of P_{max} from I_{max} differs on the results obtained with the QEOS model (see Table 1). But the differences are not large, and it is very difficult to discriminate between the two models in experiments.

Figure 9a shows the shock wave propagation in the Al layer along the Z axis as a function of time for the case of QEOS model. Figure 9b shows the shock wave propagation for the case of the RZI model. Calculations are made for the maximal intensity of laser radiation $I_{max} = 1.99 \times 10^{14}$ W/cm^2, wavelength of radiation $\lambda = 0.438$ μm and $d = 60$ μm. Here the pressure is represented as a function of the Lagrangian coordinate *XMS*, which is simply the sum of the quantities ΔM_{ij}, i.e., the mass of the Lagrangian cells in the simulation mesh.

The pressure and shock wave velocities in both models are approximately the same. For example, at $t = 0.8$ ns the maximum pressure is $P_{max} = 23.5$ Mbar for $XMS = 0.52 \times 10^{-6}$ arb. units in the case of QEOS model, and $P_{max} = 22.0$ Mbar for $XMS = 0{,}51 \times 10^{-6}$ arbitrary units in the case of the ZRI model (see Fig. 9).The pressure profile is not monotonous in case (b): this is the effect of numerical approximations. In principle, it is possible to solve this problem by decreasing the time step in the calculations. The distributions of temperature and ion charges in

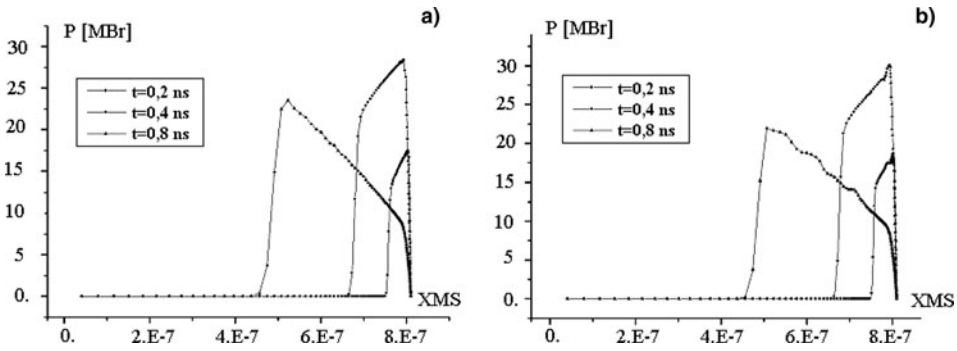

Fig. 9. The pressure distribution in the matter as function of mass cords for different time moments: $t_1 = 0.2$ ns, $t_2 = 0.4$ ns, $t_3 = 0.8$ ns (**a**) QEOS; (**b**) Zel'dovich and Raizer's EOS model.

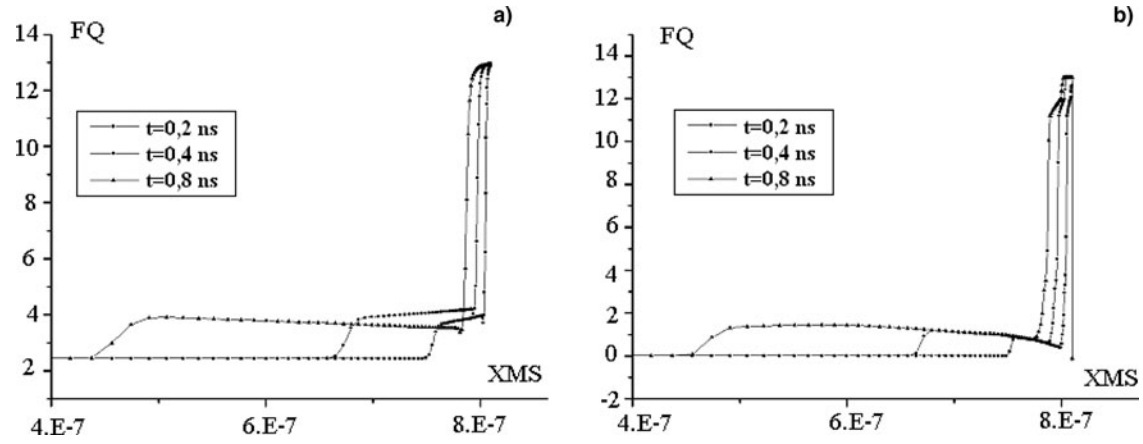

Fig. 10. Average charge of ions (FQ) as function of Lagrangian coordinates (*XM*S) for QEOS (**a**) and ZRI (**b**) models for different times. $I_{max} = 1.49 \times 10^{14}$ W/cm^2, $\lambda = 0.438$ μm.

condense matter differ some more in the QEOS and ZRI models. Figure 10 illustrates the ion charge distribution in both cases.

Figure 11 shows the evolution of the absorbed laser power as a function of distance (Z) for different times. The plotted quantity is $(P_{abs}/DM) = (P_{in} - P_{out})/DM$, where P_{in} and P_{out} are the input and output laser power in each Lagrangian cell, and DM the mass of the Lagrangian cell. In this case, the intensity of laser radiation was $I_{max} = 1.99 \times 10^{14}$ W/cm^2 and the radiation wavelength $\lambda = 0.438$ μm. The calculation shows that radiation is non-uniformly absorbed in the plasma corona, and shock wave pressure varies in time and space.

In addition, since Eq. (2) shows the dependence of pressure from time, we have also performed a set of 1D simulation to observe the dependence of P_{max} from laser pulse duration. Results are shown in Table 2. The laser pulse duration is $\tau = t_3 = 8$ ns (maximal intensity at $t_2 = 4$ ns), or, as before, $t_3 = 0.8$ ns. The range of laser intensities $I_{max} = 10^{13} - 5 \times 10^{14}$ W/cm^2, and the other parameters $\lambda = 0.438$ μm and $d = 200$ μm.

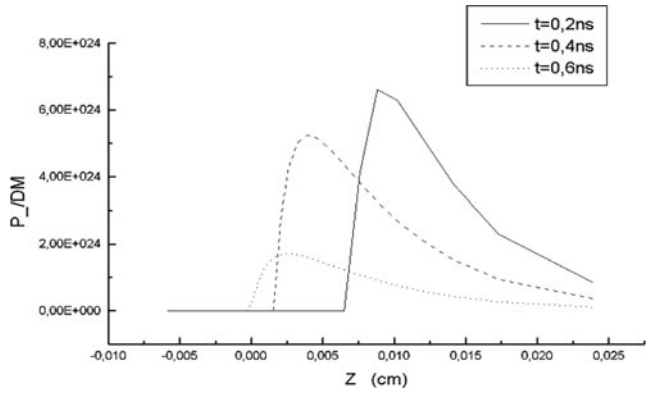

Fig. 11. Laser absorbed power per mass units (P_{abs}/DM) as function of distance (Z) for different times. $I_{max} = 1.99 \times 10^{14}$ W/cm^2, $\lambda = 0.438$ μm.

Table 2. *Comparison of two sets of numerical simulations with and $t_3 = 8$ ns and $t_3 = 0.8$ ns and the scaling for P_s given by Eq. (3). Range of laser intensities $I_{max} = 10^{13} - 5 \times 10^{14}$ W/cm^2, $\lambda = 0.438$ μm, and $d = 200$ μm*

I_{max} [10^{14} W/cm^2]	0.2	1.49	1.99	3.98
P [Mbar], $\tau = 0.8$ ns	—	22.5	28.56	50.76
P [MBar], $\tau = 8$ ns	3.234	16,37	20.83	36.38
P_s [MBar], $\tau = 0.8$ ns	4.24	22.46	28.56	50.77
P_s [Mbar], $\tau = 8$ ns	3.09	16.38	20.83	37.03

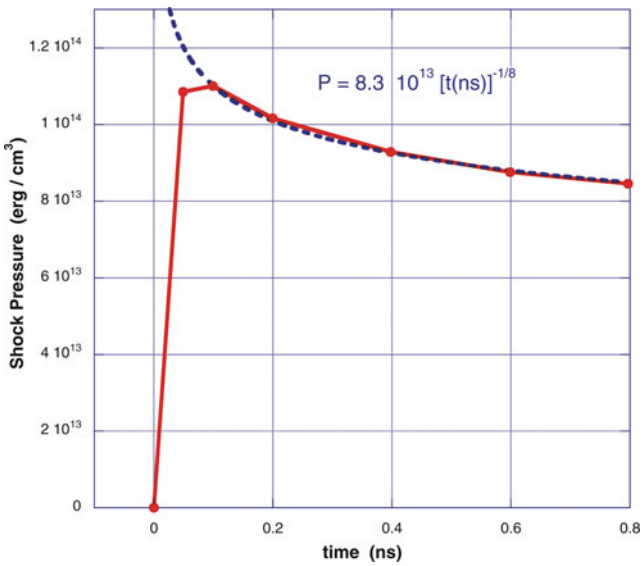

Fig. 12. (Color online) Evolution of maximum shock pressure for a laser pulse energy of 804 J, a duration of 0.8 ns (flat-top temporal shape) and an Al target with thickness 60 μm. The radius of the focal spot (used in the calculation of the laser intensity) was 200 μm. (points and solid line) and interpolation using the power law dependence of Eq. (2).

Table 3. *Shock pressure data derived from simulations (Mbar), shock velocity data calculated using Eq. (4) with $\gamma = 5/3$ (D_1) and $\gamma = 2$ (D_2), and experimental results (in km/s) for shock velocity*

I_{max}	0.995	1.1	1.2	1.5	1.99	2.2	2.98	3.98	7.96
P_S	16.06	17.46	18.8	22.6	28.56	31.04	39.9	50.8	90.25
D_1	28.1	29.4	30.3	33.2	37.4	39	44.2	49.8	66.4
D_2	29.8	31.1	32.2	35.4	39.8	41.5	47.1	53	71
D_{exp}	31	—	32.7	—	37.1	37.3	42.5	—	53

Using such results, we can improve our Eq. (6) as:

$$P_S[MBar] = 16.22 \cdot \left(\frac{I}{10^{14}[W/cm^2]}\right)^{0,83} \left(\frac{\tau}{0.8[ns]}\right)^{-0,137}. \quad (7)$$

The scaling time seems quite different from Eq. (2). However this should not be a surprise since this is the result of simulations done with varying laser intensity and for different pulse duration τ. So the physical meaning is different from Eq. (2), which shows the scaling versus time. In order to show the time dependence explicitly, we have performed a simulation using the 1D version of the code ATLANT and followed the evolution of maximum shock pressure. Results are shown in Figure 12 for laser pulse energy of 804 J and duration of 0.8 ns (flat-top temporal shape) and an Al target with thickness 60 μm.

We see that after an initial "creation" phase, shock pressure decays with time exactly as predicted by Eq. (2). We think that both these results and those presented in Figure 11, as well as the previous scaling versus laser pulse duration τ, give evidence of delocalized absorption of laser energy.

Finally we have used our simulation results to study the relation between the shock pressure (P_0) and the shock velocities (D). Classically these are related by Hugoniot equations:

$$D^2 = \frac{\gamma+1}{2}\left(\frac{P_S}{\rho_0} + \frac{\gamma-1}{\gamma+1}\frac{P_0}{\rho_0}\right), \quad (8)$$

where P_0 and ρ_o are the initial pressure and density and γ the adiabatic index. For strong shocks, as it is practically our case, this equation simplifies to

$$D^2 = \frac{\gamma+1}{2}\left(\frac{P_S}{\rho_0}\right). \quad (9)$$

Table 3 shows the relation between the laser intensity (I_{max} in units of 10^{14} W/cm^2), the pressure (P_S in Mbar), and the shock velocities for $\gamma = 5/3$ (D_1) and $\gamma = 2$ (D_2), and the experimental results (D_{exp} in km/s) (see Fig. 7). It should be noticed that laser intensity and pressure increase up to 0.4 ns and then decrease, so shock velocity varies during the laser pulse. $D_{1(2)}$ follows the maximum value of shock wave pressure.

Let's finally notice that 2D simulations have allowed predicting laser energy losses due to reflection and refraction of the laser beam in the extended plasma corona. In some cases, these can be as high as 30%. Also the pressure behind the shock front in 2D simulations with a radial profile of laser intensity tends to an asymptotic value, which is given by 1D simulations, as the width of the shock front (laser profile) is increased.

CONCLUSIONS

In this paper, we have analyzed the results of a recent experiment performed at the PALS laboratory concerning ablation pressure at 0.44 μm at irradiance up to 2×10^{14} W/cm^2, using the code "ATLANT." 2D hydrodynamics simulations have shown that 2D effects did not affect the experimental measurements of shock velocity in the conditions of "PALS" installation experiments. We have derived some scaling, which could be useful for future experiments. About 30% of laser energy was lost in the results of reflection and refraction effects. Also they allowed us to see that the shock is reasonably stationary in the step and finally give evidence of the phenomenon of delocalized absorption of laser light.

ACKNOWLEDGEMENTS

We thank all the PALS team (J. Ullschmied, J. Skala, B. Kralikova, M. Pfeifer, Ch. Kadlec, T. Mocek, and A. Präg) and C. Danson and D. Pepler from the Rutherford Appleton Laboratory, UK for the PZP.

REFERENCES

Afanas'ev, Yu., Gamaly, V., Rozanov, E.G., Trudi, V.B. (1982). The basic equations of dynamics and kinetics of laser plasma. *Trudi FIAN* **134**, pp. 32–41, Moscow, Nauka (in Russian).

Bashir, S., Rafique, M.S. & Ul-Haq, F. (2007). Laser ablation of ion irradiated CR-39. *Laser Part. Beams* **25**, 181–191.

Batani, D., Bossi, S., Benuzzi, A., Koenig, M., Faral, B., Boudenne, J.M., Grandjouan, N., Temporal, M. & Atzeni, S. (1996). Optical smoothing for shock wave generation: Application to the measurement of Equation of State. *Laser Part. Beams* **14**, 211–233.

Batani, D., Benuzzi, A., Koenig, M., Krasyuk, I., Pashinin, P., Semenov, A., Lomonosov, I., Fortov, V. (1999). Problems of

measurement of dense plasma heating in laser shock wave compression. *Laser Part. Beams* **17**, 265–274.

Batani, D., Balducci, A., Nazarov, W., Löwer, Th., Koenig, M., Faral, B., Benuzzi, A. & Temporal, M. (2001). Use of low density foams as pressure amplifiers in EOS experiments with laser driven shock waves. *Phys. Rev. E*, **63**, 46410.

Batani, D. Bleu, C. & Lower, Th. (2002). Modelistic, simulation and application of phase plates. *Euro. Phys. J D* **19**, 231.

Batani, D, Stabile, H., Ravasio, A., Desai, T., Lucchini, G., Ullschmied, J., Krousky, E., Skala, J., Kralikova, B., Pfeifer, M., Kadlec, C., Mocek, T., Prag, A., Nishimura, H., Ochi, Y., Zvorykin, V. (2003). Shock pressure induced by 0.44 μm laser radiation on aluminum. *Laser Part. Beams* **21**, 479–485.

Batani, D., Stabile, H., Ravasio, A., Desai, T., Lucchini, G., Desai, T., Ullschmied, J., Krousky, E., Juha, L., Skala, J., Kralikova, B., Pfeifer, M., Kadlec, C., Mocek, T., Präg, A., Nishimura, H., Ochi, Y. (2003). Ablation pressure scaling at short laser wavelength. *Phys. Rev. E* **68**, 067403.

Batani, D., Löwer, Th., Hall, T., Benuzzi, A. & Koenig, M. (2003). Production of high quality shocks for Equation of State Experiments. *Euro. Phys. J. D* **23**, 99.

Batani, D., Dezulian, R., Redaelli, R., Benocci, R., Stabile, H., Canova, F., Desai, T., Lucchini, G., Krousky, E., Masek, K., Pfeifer, M., Skala, J., Dudzak, R., Rus, B., Ullschmied, J., Malka, V., Faure, J., Koenig, M., Limpouch, J., Nazarov, W., Pepler, D., Nagai, K., Norimatsu, T. & Nishimura, H. (2007). Recent experiments on the hydrodynamics of laser-produced plasmas conducted at the PALS laboratory. *Laser Part. Beams* **25**, 127–141.

Bussoli, M., Batani, D., Desai, T., Canova, F., Milani, M., Trtica, M., Gakovic, B. & Krousky, E. (2007). Study of laser induced ablation with focused ion beam/scanning electron microscope devices. *Laser Particle Beams* **25**, 121–125.

Caruso, A. & Gratton, R., (1968). Some properties of the plasmas produced by irradiating light solids by laser pulses. *Plasma Phys* **10**, 867.

Fang, X. & Ahmad, S.R. (2007). Saturation effect at high laser pulse energies in laser-induced breakdown spectroscopy for elemental analysis in water. *Laser Part. Beams* **25**, 613–620.

Fortov, V.E., Kilpio, A.V., Krasyuk, I.K., Batani, D., Lomonosov, I.V., Pashinin, P.P., Shashkov, E.V., Semenov, A.Yu. & Vovchenko, V.I. (2002). The spall strength limit of matter at ultrahigh strain rates induced by laser shock wave. *Laser Part. Beams* **20**, 317–320.

Gus'kov, S.Yu., Rozanov, V.B. & Zverev, V.V. (1983). The spherical target stationary corona with allowance for fast electron transport. *Kvantovaja electronika* **10**, 802 (in Russian).

Jungwirth, K. (2005). Recent highlights of the PALS research program. *Laser Part. Beams* **23**, 177–182.

Jungwirth, K., Cejnarova, A., Juha, L., Kralikova, B., Krasa, J., Krousky, E., Krupickova, P., Laska, L., Masek, K., Mocek, T., Pfeifer, M., Prag, A., Renner, O., Rohlena, K., Rus, B., Skala, J., Straka, P., Ullschmied, J. (2001). The Prague Asterix Laser System. *Phys. Plasmas* **8**, 2495–2501.

Kato, Y., Mima, K., Miyanaga, N., Arinaga, S., Kitagawa, Y., Nakatsuka, M., Yamanaka, C. (1984). Random phasing of high-power lasers for uniform target acceleration and plasma-instability suppression. *Phys. Rev. Lett* **53**, 1057–1060.

Key, M.H., et al. (1979). Study of ablatively imploded spherical shells. *Phys. Rev. Lett* **45**, 1801.

Key, M.H., Toner, W.T., Goldsack, T.J., Kilkenny, J.D., Veats, S.A., Cunningham, P.F., Lewis, C.L.S. (1983). A study of ablation by laser irradiation of plane targets at wavelengths 1.05, 0.53, and 0.35 μm. *Phys. Fluids* **23**, 2011–2026.

Koenig, M., Fabre, E., Malka, V., Michard, A., Hammerling, P., Batani, D., Boudenne, J.M., Garconnet, J.P. & Fews, P. (1992). Recent results on implosions directly driven at $\lambda = 0.26\mu$m laser wavelength. *Laser Part. Beams* **10**, 573–583.

Koenig, M., Faral, B., Boudenne, J.M., Batani, D., Bossi, S. & Benuzzi, A. (1994). Use of optical smoothing techniques for shock wave generation in laser produced plasmas. *Phys. Rev. E* **50**, R3314–R3317.

Limpouch, J., Lebo, I.G. & Rozanov, V.B. (1987). Soviet Physics-Lebedev Institute Reports (Kratkie Soobshcheniya po Fizike: Sbornik AN SSSR, Fizicheskii Institut im P.N. Lebedeva). New York: Allerton Press Inc.

Lebo, I.G., Popov, I.V., Tishkin, V.F. & Rozanov, V.B. (1994). Two-dimensional modeling of laser-target heating and compression. *J. Russian Laser Res.* **15**, 136–143.

Lebo, I.G., Demchenko, N.N., Iskakov, A.B., Limpouch, J., Rozanov, V.B & Tishkin, V.F. (2004). Simulation of high-intensity laser-plasma interactions by use of the 2D Lagrangian code "ATLANT-HE." *Laser Part. Beams* **22**, 267–273.

Lebo, I.G. & Tishkin, V.F. (2006). Issledovanie gidrodinamicheskoy neustojchivosti v zadachah LTF. Monography, Moscow, FIZMATLIT.

Lindl, J. (1995). Development of the indirect-drive approach to inertial confinement fusion and the target physics basis for ignition and gain. *Phys. Plasmas* **2**, 3933.

Meyer, B. & Thiell, G. (1984). Experimental scaling laws for ablation parameters in plane target–laser interaction with 1.06 μm and 0.35 μm laser wavelengths. *Phys. Fluids* **27**, 302.

Mora, P. (1982). Theoretical model of absorption of laser light by a plasma. *Phys. Fluids* **25**, 1051.

More, R.M., et al. (1988). A new quotidian equation of state (QEOS) for hot dense matter. *Phys. Fluids* **31**, 3059.

Stevenson, R.M., et al. (1994). Binary-phase zone plate arrays for the generation of uniform focal profiles. *Opt. Lett*. **19**, 363.

Thareja, R.K. & Sharma, A.K. (2006). Reactive pulsed laser ablation: Plasma studies. *Laser Part. Beams* **24**, 311–320.

T4 Group LANL (1983). SESAME report on the Los Alamos Equation-of-State library. Report No. LALP-83-4. Los Alamos National Laboratory: New Mexico.

Veiko, V.P., Shakhno, E.A., Smirnov, V.N., Miaskovski, A.M. & Nikishin, G.D. (2006). Laser-induced film deposition by LIFT: Physical mechanisms and applications. *Laser Part. Beams* **24**, 203–209.

Wang, Y.L., Xu, W., Zhou, Y., Chu, L.Z. & Fu, G.S. (2007). Influence of pulse repetition rate on the average size of silicon nanoparticles deposited by laser ablation. *Laser Part. Beams* **25**, 9–13.

Zel'dovich, Y.B. & Raizer, Y.P. (1967). *Physics of Shock Waves and High Temperature Hydrodynamic Phenomena*. New York: Academic Press.